JOURNAL OF EXPERIMENTAL AND THEORETICAL PHYSICS, 2024, Vol. 166, No. 3 (9), pp. 366–373

ORDER, DISORDER, AND PHASE TRANSITION IN CONDENSED MEDIA

THE ORIGIN OF G ≈ 4 EPR LINE IN MAGNETIC NANOCOMPOSITES: MANIFESTATION OF DOUBLE QUANTUM TRANSITIONS IN FERROMAGNETIC GRANULES

© 2024 A. B. Drovosekov [a], M. Yu. Dmitrieva [a,b], A. V. Sitnikov [c,d], S. N. Nikolaev [d], V. V. Rylkov [d,e,f]

[a] Kapitza Institute for Physical Problems, Russian Academy of Sciences, Moscow, 119334 Russia
[b] National Research University Higher School of Economics, Moscow, 101000 Russia
[c] Voronezh State Technical University, Voronezh, 394026 Russia
[d] National Research Centre Kurchatov Institute, Moscow, 123182 Russia
[e] Institute of Theoretical and Applied Electrodynamics, Russian Academy of Sciences, Moscow, 125412 Russia
[f] Kotelnikov Institute of Radioengineering and Electronics, Fryazino Branch, Russian Academy of Sciences, Fryazino, Moscow oblast, 141190 Russia

* e-mail: drovosekov@kapitza.ras.ru

Received May 21, 2024
Revised May 21, 2024
Accepted May 23, 2024

Abstract. Films of metal-insulator nanogranular composites M_xD_{100-x} with different compositions and atomic percentage of metal and dielectric phases (M = Fe, Co, Ni, CoFeB; D = Al_2O_3, SiO_2, ZrO_2; x ≈ 15–60 at.%) are investigated by electron magnetic resonance in a wide range of frequencies (f = 7–37 GHz) and temperatures (T = 4.2–360 K). At concentrations of the metallic ferromagnetic phase below the percolation threshold, the experimental spectra, besides the conventional ferromagnetic resonance signal, demonstrate an additional absorption peak characterized by a double effective g-factor g ≈ 4. The appearance of such a peak in the resonance spectra and its unusual properties are explained in the framework of the quantum mechanical "giant spin" model by the excitation of "forbidden" ("double quantum") transitions in magnetic nanogranules with a change in the spin projection Δm = ±2.

Keywords: *electron magnetic resonance, magnetic nanogranular composites, giant spin model*

DOI: 10.3185ф7/S004445102409e086

1. INTRODUCTION

Magnetic nanoparticles and nanogranular systems have long been the subject of intensive research due to their unusual physical properties and wide possibilities for practical applications [1–3]. From the perspective of fundamental physics, magnetic nanoparticles can be considered as an intermediate link between paramagnetic (PM) ions and macroscopic ferromagnets. In particular, ensembles of such particles exhibit so-called superparamagnetic properties, and the magnetic dynamics of individual nanoparticles in some cases can be described within both classical and quantum approaches [4,5].

Magnetic metal-dielectric nanogranular composites (nanocomposites) represent an array of ferromagnetic (FM) nanogranules randomly distributed in a solid-state dielectric medium (matrix). In our previous works [6–10], film nanocomposites of various compositions based on transition FM metals M_xD_{100-x} based on transition FM metals M = Fe, Co, CoFeB and dielectrics D = Al_2O_3, SiO_2, $LiNbO_3$. were studied. The value x in the formula M_xD_{100-x} reflects the nominal atomic percentage of the metallic phase in the nanocomposite, a significant part of which forms FM nanogranules. At the same time, some part of the FM phase is dispersed in the form of individual

PM ions of Fe and Co в in the insulating space between granules [11,12].

In works [8–10], nanocomposite films M_xD_{100-x} were studied by magnetic resonance method in a wide range of frequencies (f = 7–37 GHz) and temperatures (T = 4.2–360 K). Besides the usual FM-resonance (FMR) signal, the experimental spectra showed an additional weaker absorption peak, characterized by an effective g-factor g » 4.3. Note that such a signal is often observed in studies of iron-based nanoparticles in various non-magnetic media [13–15] and is associated with electron PM-resonance (EPR) of isolated ions Fe^{3+}, present in the system [16–18]. In some cases, the EPR peak (g » 4.3) also manifests for ions Co^{2+} [19, 20, 21]. However, unlike traditional EPR of ions Fe^{3+}, Co^{2+}, in our case, the observed peak demonstrates a number of unusual properties:

1. it manifests much better in the longitudinal geometry of resonance excitation;

2. when changing the concentration x of the FM-phase, the nature of the temperature dependence of the peak intensity $I(T)$ changes: at low x this dependence has a decreasing character, and when approaching the percolation threshold, it becomes increasing.

We emphasize that the unusual features of the additional peak do not allow to associate it with sample composition inhomogeneity or with excitation of inhomogeneous modes of magnetic oscillations in films, as, for example, in works [22–33].

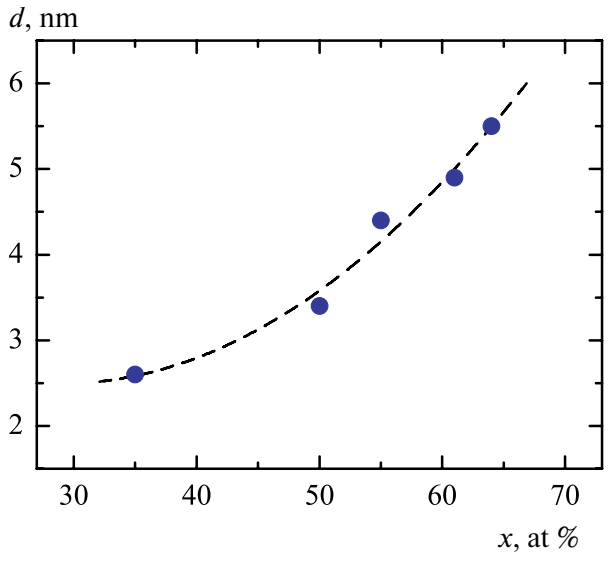

Fig 1. Average size d of FM-granules as a function of FM-phase content x in the nanocomposite $Ni_x(Al_2O_3)_{100-x}$ according to X-ray diffraction data [39]

The present work is devoted to further investigation of the nature of the anomalous magnetic resonance peak. It was found that, in addition to nanocomposites based on FM-metals Fe and Co, peak ЭПР (g » 4.3) also manifests for systems Ni_xD_{100-x} ($D = Al_2O_3$, ZrO_2) based on pure nickel. Thus, the appearance of this peak in the resonance spectra cannot be explained by the presence of isolated ions Fe^{3+} or Co^{2+} in the system. In this regard, an alternative explanation of the observed effects is proposed, suggesting a quantum mechanical approach to describing the magnetic resonance spectra of FM-nanogranules [4,5].

2. SAMPLES AND EXPERIMENTAL METHODOLOGY

Films of the nanocomposites M_xD_{100-x} with a thickness of about 1–3 μm were synthesized by ion- beam sputtering on glass-ceramic substrates using composite targets [34, 35]. The target is a plate made of FM-metal Fe, Co, Ni or alloy $Co_{40}Fe_{40}B_{20}$ (CoFeB), with a set of (12–15 pcs.) rectangular strips of oxides Al_2O_3, SiO_2 or ZrO_2. The non-uniform placement of dielectric strips on the target surface allows forming a nanocomposite film M_xD_{100-x} with smooth controlled concentration variation x along the substrate in a wide range of Dx » 30–40 ат. %. Further studies are conducted on small pieces of grown film with dimensions of 5′ 5 mm^2, so that the variation of x within one sample is less than 1 at. %. The content of the metallic phase in the films was determined by energy-dispersive X-ray microanalysis.

According to transmission electron microscopy and X-ray diffraction data, the obtained composites represent an ensemble of crystalline FM-nanogranules randomly distributed within an amorphous oxide matrix [35–40]. The granules have a near-circular shape, and their average size (2–8 nm) gradually increases with the growth of FM-phase content in the nanocomposite (Fig. 1).

The percolation threshold for all studied composites lies in the vicinity of metallic phase concentrations of $x \simeq 50$ at. %. According to magnetic data, approximately in the same concentration range or slightly lower, the samples show transition

from superparamagnetic to ferromagnetic behavior [33-39].

In the present work, nanocomposite samples are studied by magnetic resonance method in a wide range of frequencies (f = 7–37 GHz) and temperatures (T = 4.2–360 K) using a laboratory transmission-type spectrometer based on rectangular and tunable cylindrical resonators [8]. In the measurement geometry used, the external static magnetic field **H** (up to 17 kOe) lies in the film plane. It is possible to orient the high-frequency magnetic field **h** both perpendicular (**h** ⊥ **H**), and parallel (**h** ∥ **H**) to the static field ("transverse" and "longitudinal" resonance excitation geometries).

3. EXPERIMENTAL RESULTS

Figures 2,3 show experimental magnetic resonance spectra obtained for a series of studied nanocomposites M_xD_{100-x} at room temperature. In the conventional transverse geometry of resonance excitation (**h** ⊥ **H**) an intense FMR absorption peak is observed for all structures. As shown previously [6, 8, 10], the frequency-field diagrams for this peak, as well as the dependence of its position on the field orientation relative to the film plane, are well described by conventional Kittel formulas taking into account the demagnetizing factor $4\pi M$.

When changing the resonance excitation geometry to longitudinal (**h** ∥ **H**), the FMR peak intensity decreases significantly. In this case, a second absorption peak appears in a weaker field. In works it was demonstrated that the frequency-field and orientation dependences for this peak are well described by a simple EPR formula

$$f = \gamma H_{eff}, \qquad (1)$$

where the gyromagnetic ratio γ corresponds to the effective g-factor $g = 4.3 \pm 0.1$, and the effective field H_{eff}, in addition to the external field, includes magnetodipole fields created inside the film by an array of FM granules.

Note that the (g » 4) EPR peak appears in systems of various compositions, including nanocomposites based on pure Co and Ni which prevents associating it with traditional EPR ions Fe^{3+} (g » 4.3). At the same time, it can be noted that the observed effective g-factors for FMR and EPR peaks differ by approximately 2 times. For the FMR line, depending on the film composition, the

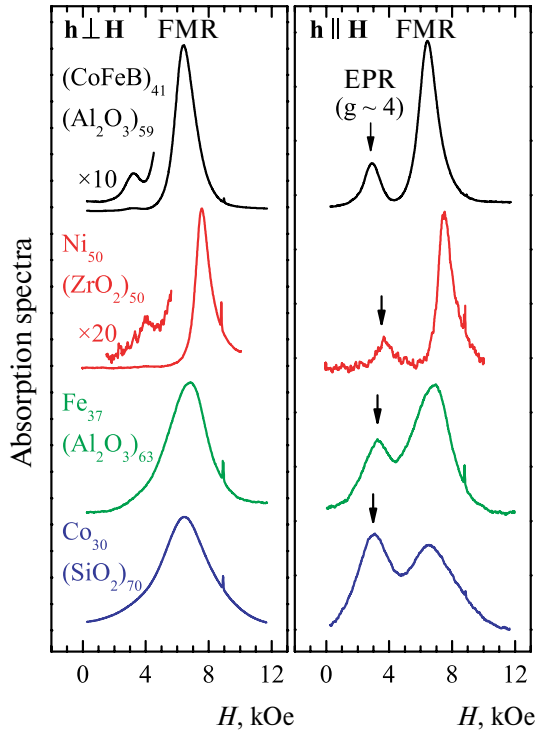

Fig. 2. Magnetic resonance spectra in nanocomposite films of different compositions M_xD_{100-x} in transverse (**h** ⊥ **H**) and longitudinal (**h** ∥ **H**) excitation geometry. The spectra were obtained at a frequency of $f \approx 25$ GHz at room temperature

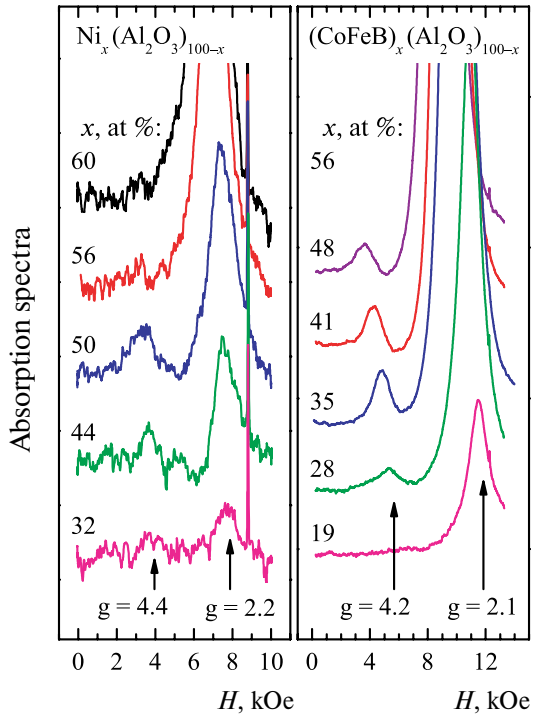

Fig. 3. Experimental spectra for nanocomposite films $Ni_x(Al_2O_3)$ at frequency $f \approx 24.6$ GHz and $(CoFeB)_x(Al_2O_3)_{100-x}$, ($f \approx 34.4$ GHz) obtained at room temperature in longitudinal resonance excitation geometry (**h** ∥ **H**)

g-factor varies in the range of g » 2.1–2.2, which is characteristic for metallic Fe, Co, Ni and their alloys [41]. For the EPR line, this value turns out to be 2 times larger: g » 4.2–4.4.

As an example, Fig. 4 shows frequency-field diagrams for two resonance peaks in Ni-based nanocomposites. In the high-frequency region, the dependencies. $f(H)$ are described by linear functions whose slopes differ by a factor of 2.

Note that the narrowest resonance peaks are observed for films $(CoFeB)_x(Al_2O_3)_{100-x}$ and Ni_xD_{100-x}. For these structures, the EPR peak (g » 4) can be resolved in both longitudinal and transverse resonance excitation geometries (see Fig.2). Moreover, its amplitude turns out to be approximately the same in both geometries [8, 10].

Another unusual feature of the EPR peak (g » 4) is the anomalous dependence of its intensity on the FM-phase content in the nanocomposite (see Fig. 3) and temperature (Fig. 5–7). Note that the main FMR peak behaves quite naturally in this respect — its intensity monotonically increases with increasing concentration of FM-phase and with temperature decrease. A different pattern is observed for the EPR peak. Spectra measured at room temperature demonstrate non-monotonic behavior of the EPR peak intensity (g » 4) on FM-phase content in the nanocomposite, x (Fig.3). With increasing x the peak first grows, however, when crossing the percolation threshold x ‰50 % decreases and disappears.

When changing the FM-phase content in the nanocomposite, the character of the temperature dependence of the EPR peak intensity also changes (Fig.5-7). At low FM-phase concentrations x ˆ 25 at. % the peak intensity $I(T)$ monotonically increases with decreasing temperature according to the usual Curie law $I(T)$ µ $1/T$. However, with increasing x the dependence $I(T)$ becomes non-monotonic with the presence of a temperature maximum. As increases, the intensity maximum shifts to higher temperatures. Finally, in the limit of high FM-phase concentrations, only approximately linear growth $I(T)$ µ T (Fig. 6) [9] is observed.

4. "GIANT SPIN" MODEL

The appearance of a resonance peak with doubled effective g-factor in the spectra can be explained within the "giant spin" model by the excitation of "double-quantum" transitions with a change in spin projection Dm = ± 2 [42–46] inside FM-nanogranules. Within this approach, one can explain the more pronounced manifestation of the peak with g » 4 in the longitudinal geometry of resonance

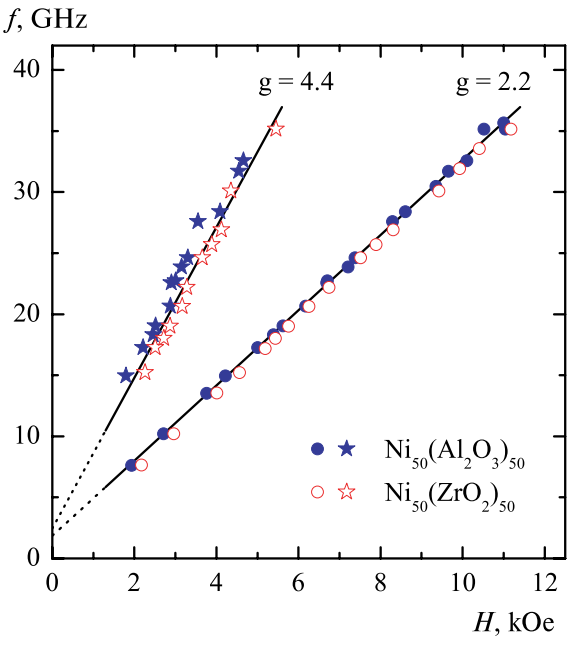

Fig. 4. Frequency-field dependencies for two resonance peaks in films $Ni_{50}(Al_2O_3)_{50}$ and $Ni_{50}(ZrO_3)_{50}$ at room temperature. Symbols — experimental data, the slope of straight lines corresponds to effective g-factors g = 2.2 and g = 4.4

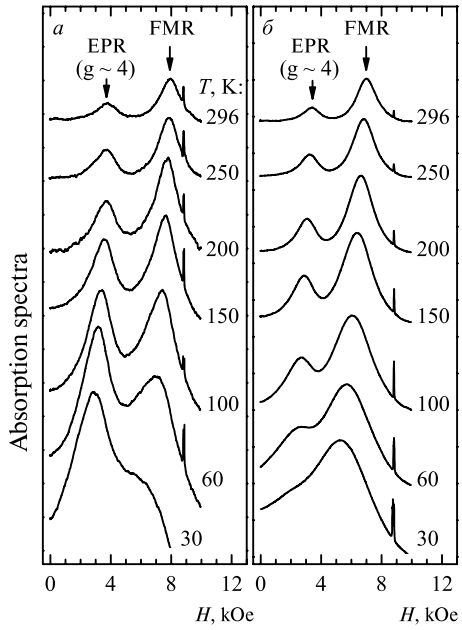

Fig. 5. Spectra of films $(CoFeB)_x(Al_2O_3)_{100-x}$ with concentration x ≈ 25 at. % (*a*), 35 at. % (*b*) at different temperatures T = 30–29.6 K, obtained at frequency f ≈ 25 GHz in longitudinal resonance excitation geometry (**h** || **H**)

excitation [44–46], as well as the anomalous temperature dependence of its intensity [42, 44, 45].

In the giant spin model, an FM-nanogranule is treated as a PM-center with a very large spin $S \sim 10^2$–10^4. In an external field, Zeeman splitting of the energy levels of this spin occurs according to its projection on the field direction $m = -S \ldots +S$. Forced transitions with a change in spin projection $\Delta m = \pm 1$ under the action of an alternating field in the classical limit correspond to the excitation of the usual FMR mode. Nominally "forbidden" ("double-quantum") transitions with $\Delta m = \pm 2$ become "allowed" taking into account additional perturbations in the system, for example, in the presence of magnetic anisotropy of granules or dipole-dipole interactions between them [19, 47].

Let's consider the simplest case of weak uniaxial anisotropy of granules with effective field H_A. Such anisotropy can arise in granules, for example, when their shape deviates from spherical. In this case, the quantum mechanical probability of transitions between levels $m \pm 1$ of the granule within perturbation theory is estimated by the expression [48, 49]

$$f_{m\pm1} \propto \left(\frac{H_A}{H}\right)^2 \frac{(U_m^{m-1}U_{m+1}^{m})^2}{S^2}, \qquad (2)$$

where

$$U_m^{m-1} = \sqrt{S(S+1) - m(m-1)}.$$

Note that for arbitrary orientation of the anisotropy axis relative to the field direction, the probabilities of excitation of such transitions by transverse and longitudinal variable fields are comparable [49], which agrees with the experimentally observed behavior of the g ≈ 4 EPR peak.

Note that according to formula (2), near the ground state of the granule, $m = -S$, the probability of transitions with $\Delta m = \pm 2$ tends to zero. Conversely, the maximum probabilities of these transitions are realized at small values of $|m| = S$. However, the corresponding energy levels lie above the ground state $m = -S$ by a value of the order of μH, where μ is the magnetic moment of the granule. Therefore, under low temperature conditions ($k_B T \ll \mu H$, k_B is Boltzmann constant), when granules transition to the ground state, the intensity of the "double-quantum" line $I(T)$ decreases. In the limit of high temperatures

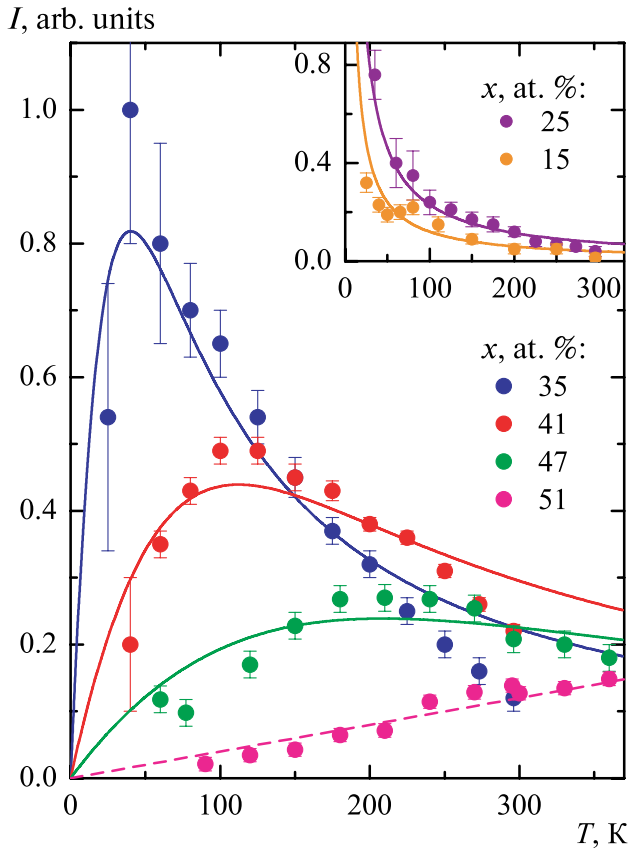

Fig. 6. Temperature dependencies of integral intensity $I(T)$ of EPR line ($g \approx 4$) for nanocomposite films $CoFeB)_x(Al_2O_3)_{100-x}$. Symbols are the experimental data at frequency $f \approx 25$ GHz, solid lines are calculation in the "giant spin" model, dashes — linear dependence. Lines in the inset are the Curie law $I(T) \propto 1/T$

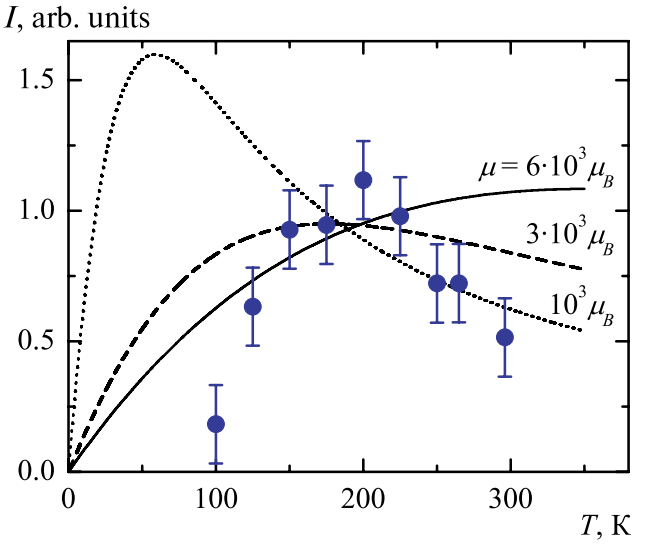

Fig. 7. Temperature dependence of the integral intensity $I(T)$ of the EPR line ($g \approx 4$)) for the film $Ni_{50}(Al_2O_3)_{50}$. Symbols are the experimental data at frequency $f \approx 18$ GHz, lines are calculation in the "giant spin" model with different values of magnetic moment of granules μ

($k_BT \gg \mu H$) the equalization of the granule energy level populations leads to the dependence $I(T)$ following Curie's law $I(T) \mu 1/T$. Thus, the maximum line intensity with $g \approx 4$ is expected at temperature $T \sim \mu H/k_B$. With increasing FM-phase concentration in the nanocomposite, the magnetic moment of granules grows, which explains the maximum shift to higher temperatures. Above the percolation threshold, granules begin to merge into macroscopic clusters, π sharply increases, and the double-quantum line completely disappears.

For quantitative evaluation of line intensity, let's consider the difference in level populations $m \pm 1$ at finite temperature T:

$$\Delta p_{m\pm1}(T) = Z_S^{-1}\left(e^{-2(m-1)\omega} - e^{-2(m+1)\omega}\right),$$

where Z_S is the partition function, given by the known expression [50]

$$Z_S = \frac{\sinh[(2S+1)\omega]}{\sinh(\omega)}, \qquad \omega = \frac{\mu_B H_{eff}}{k_B T}$$

(μ_B is the Bohr magneton). The effective field H_{eff} in the above equations, besides the external field, includes magnetodipole fields created inside the film by the FM-granule array. According to formula (1), this field is determined by the simple relation $H_{eff} = f/\gamma$. Taking into account the probabilities of double-quantum transitions (2), the integral intensity of the EPR line ($g \approx 4$) is proportional to

$$I(T) \mu \sum_{m=1-S}^{S-1} f_{m\pm1}\Delta p_{m\pm1}(T). \qquad (3)$$

Figures 6,7 present a comparison of experimental dependencies $I(T)$ for the EPR peak ($g \approx 4$) in films of different compositions with the results of numerical calculations in the described model. The fitting parameters are the vertical scale of function (3) and the particle spin S (corresponding magnetic moment $\mu = 2S\mu_B$), which determines the position of maximum $I(T)$ by temperature.

At a qualitative level, the experimental data are consistent with the theory. However, systematic quantitative discrepancies can be observed. Compared to calculations, the experimental dependencies $I(T)$ demonstrate sharper maxima. This discrepancy is more pronounced for the Ni-based nanocomposite (Fig.7). As shown in Fig. 7, the observed behavior can be formally attributed to the decrease in magnetic moment of π granules with increasing temperature. Indeed, considering the finite Curie temperature T_C of the granule material, under the conditions $T \lesssim T_C$ the reduction effect π(T) is quite expected. In the case of Ni granules, this effect should be more pronounced due to lower T_C compared to CoFeB. Note also that as temperature decreases, magnetic interactions between nanogranules may play an important role and lead to the formation of larger magnetically ordered clusters, causing additional growth in the effective value of π [51]. [51]. However, the considered simplest model completely neglects such effects of intergranular interactions and does not account for the presence of excited states of nanoparticles with reduced total spin value at $T \lesssim T_C$, and therefore is only a qualitative approximation of the real situation.

Figure 8 shows the results of estimating the magnetic moment μ of granules from the dependencies $I(T)$ for the EPR peak ($g \approx 4$) in films $(CoFeB)_x(Al_2O_3)_{100-x}$. For comparison, the values based on the Langevin function approximation of curves $4\pi M(H)$, obtained from FMR data at room temperature, as described in work [10].

As can be seen, the granule magnetic moment values determined by two methods are of the same order. However, EPR data systematically show lower values π compared to FMR data. It can be assumed that this difference is due to the size distribution of FM granules. In this case, the FMR peak is mainly

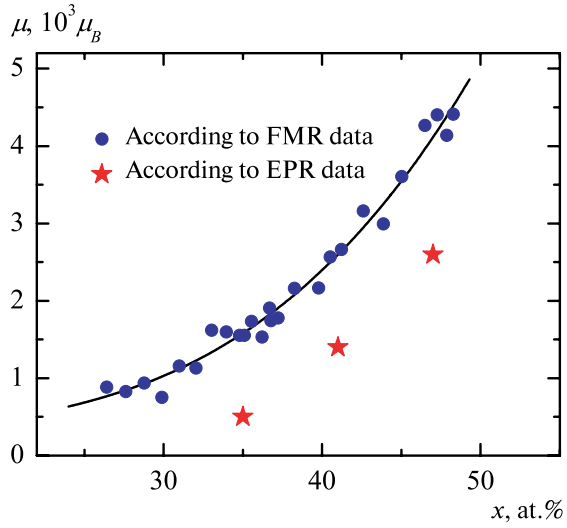

Fig. 8. Granule magnetic moment as a function of FM phase concentration in nanocomposite $(CoFeB)x(Al_2O_3)_{100-x}$, obtained from the approximation of dependencies $4\pi M(H)$ (from FMR data) and from temperature dependencies of EPR peak intensity

determined by resonance in large granules, while the EPR peak (g » 4) is more effectively excited in small magnetic particles.

5. CONCLUSION

Films of metal-insulator nanogranular composites M_xD_{100-x} with various compositions (M = Fe, Co, Ni, CoFeB; D = Al_2O_3, SiO_2, ZrO_2) and contents of the metallic FM phase $x \approx 15-60$ at. % were studied by electron magnetic resonance. The experimental spectra, in addition to the usual FMR signal, contain an additional absorption peak with doubled effective g-factor g » 4, demonstrating a number of unusual features. The appearance of such a peak in the spectra and its properties can be explained within the quantum mechanical "giant spin" model, considering FM-nanogranules as PM-centers with a very large spin $S \sim 10^2-10^4$. The observed EPR line (g » 4) is associated with the excitation of double-quantum transitions in these PM-centers with a change in spin projection $\Delta m = \pm 2$. The proposed approach makes it possible to explain qualitatively the non-monotonic temperature dependence of the unusual peak intensity, non-standard conditions of its excitation by longitudinal high-frequency magnetic field, and the disappearance of the peak at FM-phase content above the percolation threshold of the nanocomposite.

Thus, the observed features of magnetic resonance in nanogranular composites emphasize the "dualism" of classical and quantum properties of FM-nanoparticles. The behavior of the main FMR line is well described within the classical concepts of exciting precession of the magnetization vector in the nanogranule ensemble. At the same time, the properties of the additional peak are explained in quantum mechanical terms by the excitation of EPR transitions between spin states of individual nanogranules.

FUNDING

The work was carried out within the State Assignment with support from the Russian Science Foundation (project No. 22-19-00171).

REFERENCES

1. Magnetic Properties of Fine Particles, ed. by J. L. Dormann and D. Fiorani (Elsevier, Amsterdam, 1992).
2. Magnetic Nanoparticles, ed. by S. P. Gubin (Wiley, Hoboken, NJ, 2009).
3. S. Bedanta, A. Barman, W. Kleemann, O. Petracic, and T. Seki, J. Nanomater. 2013, 952540 (2013).
4. N. Noginova, F. Chen, T. Weaver, E. P. Giannelis, A. B. Bourlinos, and V. A. Atsarkin, J. Phys.: Cond. Mat. 19, 246208 (2007).
5. V. A. Atsarkin and N. Noginova, Appl. Magn. Reson. 51, 1467 (2020).
6. A. B. Drovosekov, N. M. Kreines, A. S. Barkalova, S. N. Nikolaev, V. V. Rylkov, and A. V. Sitnikov, J. Magn. Magn. Mater. 495, 165875 (2020).
7. A. B. Drovosekov, N. M. Kreines, A. S. Barkalova, S. N. Nikolaev, A. V. Sitnikov, and V. V. Rylkov, JETP Lett. 112, 84 (2020).
8. A. B. Drovosekov, N. M. Kreines, O. A. Kovalev, A. V. Sitnikov, S. N. Nikolaev, and V. V. Rylkov, J. Exp. Theor. Phys. 134, 725 (2022).
9. A. B. Drovosekov, N. M. Kreines, O. A. Kovalev, A. V. Sitnikov, S. N. Nikolaev, and V. V. Rylkov,J. Exp. Theor. Phys. 135, 372 (2022).
10. A. B. Drovosekov, N. M. Kreines, D. A. Ziganurov, A. V. Sitnikov, S. N. Nikolaev, and V. V. Rylkov, J. Exp. Theor. Phys. 137, 562 (2023).
11. V. Rylkov, A. Sitnikov, S. Nikolaev, A. Emelyanov, K. Chernohlazov, K. Nikiruy, A. Drovosekov, M. Blinov, E. Fadeev, A. Taldenkov, V. Demin, A. Vedeneev, A. Bugaev, and A. Granovsky, IEEE Magnetics Letters 10, 2509504 (2019).
12. V. V. Rylkov, A. V. Emelyanov, S. N. Nikolaev, K. E. Nikiruy, A. V. Sitnikov, E. A. Fadeev, V. A. Demin, and A. B. Granovsky, J. Exp. Theor. Phys. 131, 160 (2020).
13. Yu. A. Koksharov, D. A. Pankratov, S. P. Gubin, I. D. Kosobudsky, M. Beltran, Y. Khodorkovsky, and A. M. Tishin, J. Appl. Phys. 89, 2293 (2001).
14. A. Jitianu, M. Crisan, A. Meghea, I. Rau, and M. Zaharescu, J. Mater. Chem. 12, 1401 (2002).
15. I. Edelman, O. Ivanova, R. Ivantsov, D. Velikanov, V. Zabluda, Y. Zubavichus, A. Veligzhanin, V. Zaikovskiy, S. Stepanov, A. Artemenko, J. Curély, and J. Kliava, J. Appl. Phys. 112, 084331 (2012).
16. T. Castner, G. S. Newell, W. C. Holton, and C. P. Slichter, J. Chem. Phys. 32, 668 (1960).
17. H. H. Wickman, M. P. Klein, and D. A. Shirley, J. Chem. Phys. 42, 2113 (1965).
18. Ya. G. Kliava, EPR Spectroscopy of Disordered Solids (Zinatne, Riga, 1988) [in Russian].
19. A. Abragam and B. Bleaney, Electron paramagnetic resonance of transition ions (Clarendon Press, Oxford, 1970).

20. C. Legein, J. Y. Buzaré, and C. Jacoboni, J. Non-Cryst. Solids 161, 112 (1993).

21. O. Raita, A. Popa, D. Toloman, M. Stan, A. Darabont, and L. Giurgiu, Appl. Magn. Reson. 40, 245 (2011).

22. W. Wang, Z. Jiang, and Y. Du, J. Appl. Phys. 78, 6679 (1995).

23. N. A. Lesnik, R. Gontarz, G. N. Kakazei, A. F. Kravets, P. E. Wigen, and J. Dubowik, Phys. Stat. Sol. (a) 196, 157 (2003).

24. J. Gómez, A. Butera, and J. A. Barnard, Phys. Rev. B 70, 054428 (2004).

25. G. N. Kakazei, Yu. G. Pogorelov, M. D. Costa, V. O. Golub, J. B. Sousa, P. P. Freitas, S. Cardoso, and P. E. Wigen, J. Appl. Phys. 97, 10A723 (2005).

26. M. J. M. Pires, J. C. Denardin, E. C. da Silva, and M. Knobel, J. Appl. Phys. 99, 063908 (2006).

27. S. A. Vyzulin, Yu. E. Kalinin, G. F. Kopytov, E. V. Lebedeva, A. V. Sitnikov, and N. E. Syr'ev, Russ. Phys. J. 49, 285 (2006).

28. G. N. Kakazei, X. M. Liu, J. Ding, V. O. Golub, O. Y. Salyuk, R. V. Verba, S. A. Bunyaev, and A. O. Adeyeye, Appl. Phys. Lett. 107, 232402 (2015).

29. O. N. Martyanov, D. A. Balaev, O. V. Pylypenko, L. V. Odnodvorets, S. V. Chernov, S. A. Nepijko, H. J. Elmers, C. M. Schneider, and G. Schönhense, J. Supercond. Nov. Magn. 28, 3587 (2015).

30. E. N. Kablov, O. G. Ospennikova, V. P. Piskorskii, D. V. Korolev, Yu. E. Kalinin, A. V. Sitnikov, E. I. Kunitsyna, A. D. Talantsev, V. L. Berdinskii, and R. B. Morgunov, Phys. Solid State 58, 1121 (2016).

31. N. Neugebauer, A. Fabian, M. T. Elm, D. M. Hofmann, M. Czerner, C. Heiliger, and P. J. Klar, Phys. Rev. B 101, 104409 (2020).

32. L. N. Kotov, M. P. Lasek, V. K. Turkov, D. M. Kholopov, V. S. Vlasov, Yu. E. Kalinin, and A. V. Sitnikov, Bull. Russ. Acad. Sci. Phys. 84, 1065 (2020).

33. E. A. Denisova, S. V. Komogortsev, R. S. Iskhakov, L. A. Chekanova, Yu. E. Kalinin, and A. V. Sitnikov, Acta Physica Polonica A 134, 623 (2018).

34. O. V. Stognei, A. V. Sitnikov, and A. J. Al-Maliky, Bull. Voronezh State Technical University 10, 7 (2014) [in Russian].

35. Yu. E. Kalinin, A. V. Sitnikov, and O. V. Stognei, International Scientific Journal for Alternative Energy and Ecology 54, 9 (2007) [in Russian].

36. V. V. Rylkov, S. N. Nikolaev, K. Yu. Chernoglazov, V. A. Demin, A. V. Sitnikov, M. Yu. Presnyakov, A. L. Vasiliev, N. S. Perov, A. S. Vedeneev, Yu. E. Kalinin, V. V. Tugushev, and A. B. Granovsky, Phys. Rev. B 95, 144202 (2017).

37. O. V. Stognei and A. V. Sitnikov, Phys. Solid State 52, 2518 (2010).

38. I. M. Tregubov, M. Yu. Smolyakova, D. N. Klimenko, M. A. Kashirin, and O. V. Stognei, Russ. J. Non-ferrous Metals 2, 37 (2013) [in Russian].

39. [39] O. V. Stognei, A. J. Maliki, A. A. Grebennikov, K. I. Semenenko, E. O. Bulovatskaya, and A. V. Sitnikov, Semiconductors 50, 709 (2016).

40. M. S. Filatov, O. V. Stognei, and M. S. Antonova, J. Phys. Conf. Ser. 872, 012029 (2017).

41. M. A. W. Schoen, J Lucassen, H. T. Nembach, T. J. Silva, B. Koopmans, C. H. Back, and J. M. Shaw, Phys. Rev. B 95, 134410 (2017).

42. N. Noginova, T. Weaver, E. P. Giannelis, A. B. Bourlinos, V. A. Atsarkin, and V. V. Demidov, Phys. Rev. B 77, 014403 (2008).

43. N. Noginova, B. Bates, and V. A. Atsarkin, Appl. Magn. Reson. 47, 937 (2016).

44. M. Fittipaldi, R. Mercatelli, S. Sottini, P. Ceci, E. Falvo, and D. Gatteschi, Phys. Chem. Chem. Phys. 18, 3591 (2016).

45. A. Cini, P. Ceci, E. Falvo, D. Gatteschi, and M. Fittipaldi, Z. Phys. Chem. 231, 745 (2017).

46. N. E. Domracheva, V. E. Vorobeva, M. S. Gruzdev, Y. N. Shvachko, and D. V. Starichenko, Inorganica Chimica Acta 465, 38 (2017).

47. S. A. Altshuler and B. M. Kozyrev, Electron Paramagnetic Resonance in Compounds of Transition Elements (Wiley, New York, 1974; Nauka, Moscow, 1972).

48. C. Marti, R. Romestain, and R. Visocekas, Phys. Stat. Sol. 28, 97 (1968).

49. B. Clerjaud, Phys. Stat. Sol. (b) 72, K33 (1975).

50. J. S. Smart, Effective field theories of magnetism (Saunders, London, 1966).

51. S. N. Nikolaev, K. Yu. Chernoglazov, A. V. Emelyanov, A. V. Sitnikov, A. N. Taldenkov, T. D. Patsaev, A. L. Vasiliev, E. A. Gan'shina, V. A. Demin, N. S. Averkiev, A. B. Granovsky, and V. V. Rylkov, JETP Letters 118, 58 (2023).